Supplementary Information: An objective method for the assessment of fluid injection induced seismicity and application to tectonically active regions in central California

T. H. W. Goebel[1], E. Hauksson[1], F. Aminzadeh[2], and J.-P. Ampuero[1]

[1]Seismological Laboratory, California Institute of Technology, Pasadena, California, USA.
[2]Department of Chemical Engineering, University of Southern California, Los Angeles, California, USA.

Contents

Additional Supporting Information (Files uploaded separately)

1. Goebel_JGR_catalog_01.txt - seismicity catalog
2. Goebel_JGR_inj_rate_Bv_02.txt - injection rates
3. Goebel_JGR_inj_rate_Kr_b_03.txt - injection rates
4. Goebel_JGR_inj_rate_Lh_b1_04.txt - injection rates
5. Goebel_JGR_inj_rate_Tj_b_05.txt - injection rates
6. Goebel_JGR_inj_rate_Ex1_SI_06.txt - injection rates
7. Goebel_JGR_inj_rate_Ex2_SI_07.txt - injection rates
8. Goebel_JGR_well_location_08.txt - well locations

1 Introduction

Within this supplementary material, we provide a simple flow chart and two detailed examples of applying the OISC method to specific injection and seismicity data sets. We then explore significance tests and evaluate the characteristics of R-ratios for different synthetic earthquake catalogs. Lastly, we show the depth distributions of the four cases of likely induced seismicity discussed in the main manuscript.

2 OISC-method flow chart

The following flow-chart displays data sets and analysis steps that are part of the OISC-method (Figure 1). Starting from the input data, the chart shows the three basic analysis steps, followed by a decision module. This decision module uses the computed statistical measures (i.e. P_{poi}, P_{ran}, $\overline{R}$ and p), that quantify the short-term correlation between seismicity and injection rate changes, to discriminate likely fluid-injection induced from tectonic earthquake sequences based on the selected thresholds. The module that identifies possible earthquake triggers, here type-a and b triggers, can be changed to include other suitable criteria such as total injected volumes or net-production rates. All of the statistical tests for the evaluation of injection and seismicity correlations can then still be used to evaluate the significance of the correlations.

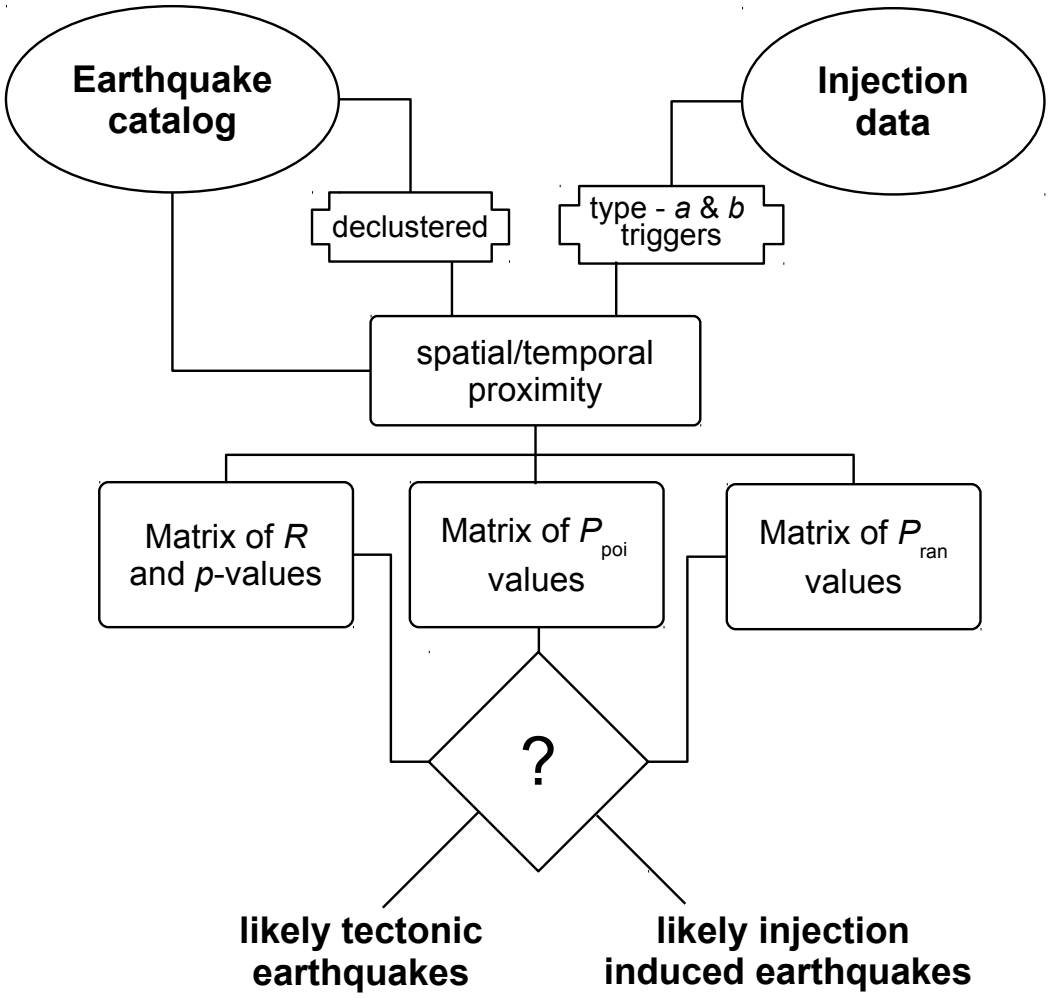

Figure 1: Flow chart highlighting the required data and analysis steps for the OISC method. The statistical measures P_{poi}, P_{ran}, $\overline{R}$ and p are computed for all trigger IDs and injection thresholds resulting in a matrix of values from which likely induced sequences can be identified.

3 Example application of the OISC method

Figure 2a displays an example for which the start of fluid-injection in a disposal well is apparently correlated with an increase in seismicity rates after ∼1986. In addition, a second rapid increase in injection rates between 1987 and 1988 is followed by an increase in seismicity rates and a $M_L > 3$ event. However, when considering the entire duration of the recorded seismic and injection activity (Figure 2b), this brief period of correlated behavior appears insignificant in contrast to the continuous increase in injection rates until 1993 and lack of seismic activity. Moreover, at least one earthquake sequence occurred within the area before injection commenced.

We use the seismicity and injection activity in Figure 2 to present a detailed application of the OISC method. We conduct this analysis for a comparably short (8 years, i.e. 1986-1994) and a longer period (37 years, i.e. 1977-2014) to examine the influence of observational window length when establishing the baseline for background injection and seismic activity. This baseline is essential for the evaluation of the statistical significance of the results. The steps below explain the application of the OISC method in detail and follow Section 4.6 in the main manuscript:

1. We start by determining trigger onsets for specific types of well injection activity. For the present example we chose type-b triggers with a change in monthly injection rates of 200 kbbl/mo. This results in 4 trigger onsets for the 8 year time period and 7 trigger onsets for the 37 year time period.

2. We then select seismic events within a specific space, time window (here $r = 15.45$ km, $\Delta t = 110$ days) close to the well location and each trigger onset. This results in the selection of 214 events with 1 above M3 for a 8 year period and 429 events with 2 above M3 for a 37 year period. During the short observational period, the only trigger onset that is associated with seismicity above M3 within the space-time window is the abrupt change in fluid injection activity at t = 1986.53.

   We now determine the significance of correlations within the two observational periods. The failure of any one of the following significance tests results in the rejection of the hypothesizes that seismicity is connected to nearby injection activity.

3. Based on the rate of independent mainshocks within r of injection for the 8 and 37 year observational periods the Poissonian probabilities of observing one $M3$ event in a 110 day window and at a distance of 15.45 km is 0.018 for the 8 year period and 0.013 for the 37 year period.

4. We now test if the episodes of type-b injection activity and $M3$ earthquake sequences coincide by chance using Equ. (4) in the main manuscript. For the 8 year observational period, we determine a value of P_{ran}=0.018 and for the 37 year long catalog, we get a value of P_{ran}=0.09. This shows that there is an almost 10 % probability to observe an earthquake sequence above $M3$ within the selected space/time window by random chance. The relative increase in P_{ran} between the 8 and 37 year period underlines that type-b triggers and seismic sequences above $M3$ are a lot more common than would be expected from the 8 year observational period.

5. The last test evaluates if there is a significant increase in the rates of events at the time of the trigger onset using the R-statistic. In contrast to P_{poi}, this test does not require a pre-selection of earthquakes according to magnitude and compares the pre to the post trigger seismicity without the strong sensitivity to the selected space/time window. For the 8 year period, we determine a value of R=0.43 (0.36, 0.52) with a p-value of 0.18, and for the 37 year period R= 0.43, (0.38, 0.47) with a p-value of 0.15. The R-ratio results show that there is an increase in seismicity rates following the trigger onset in 1986 but this increase is not significant on short and long time scales considering the overall rate variability within the region.

Steps 2 to 5 are repeated in the main manuscript for all injection wells and for varying injection rates between 10 and 600 kbbl. The present example shows the significance tests of spatial/temporal association between injection and seismic activity should be based on sufficiently long time windows.

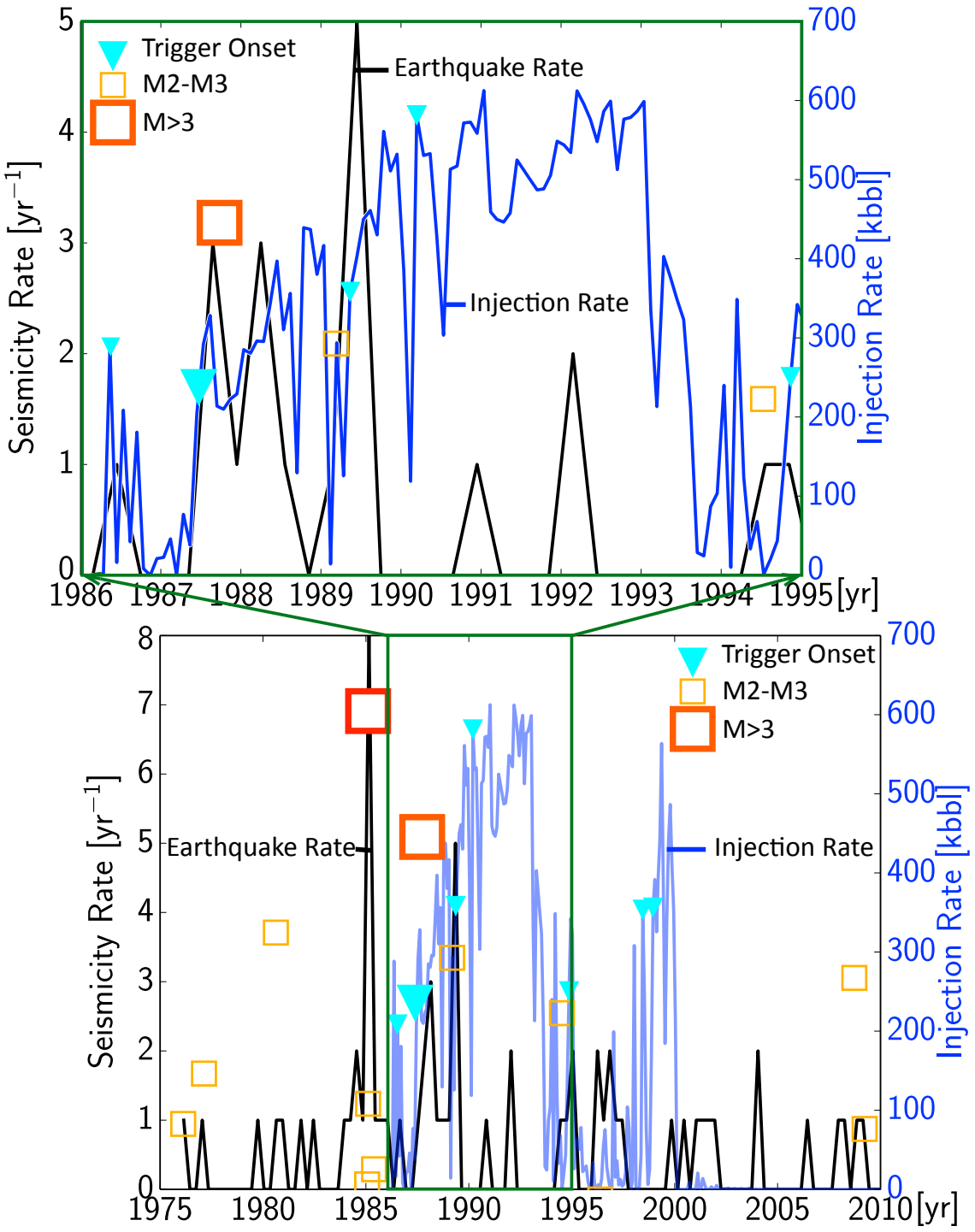

Figure 2: Upper: Example of injection (blue curve) and seismic activity (black curve, binned every 0.3 yr) at a short time-scale suggesting a possible correlation between the two. *M*2 and *M*3 earthquakes are shown by yellow and red squares, Trigger onsets, corresponding to type-b injection activity of 200 kbbl or more are shown by cyan triangles, with a large triangle depicting a trigger onset that is closely followed by M>3 event. Lower: Same as above but now for a longer period. The commencement of fluid injection likely did not alter the seismicity within the region. This example highlights the importance of long enough seismicity records to establish statistically significant correlations.

Table 1: Results of statistical evaluation of injection and seismicity in Figure 2.

	1986–1994	**1977–2014**
No. of Triggers	4	7
P_{poi}	0.015	0.013
P_{ran}	0.018	0.09
R	0.43 (0.36, 0.52)	0.43 (0.38, 0.47)
p-value	0.15	0.18

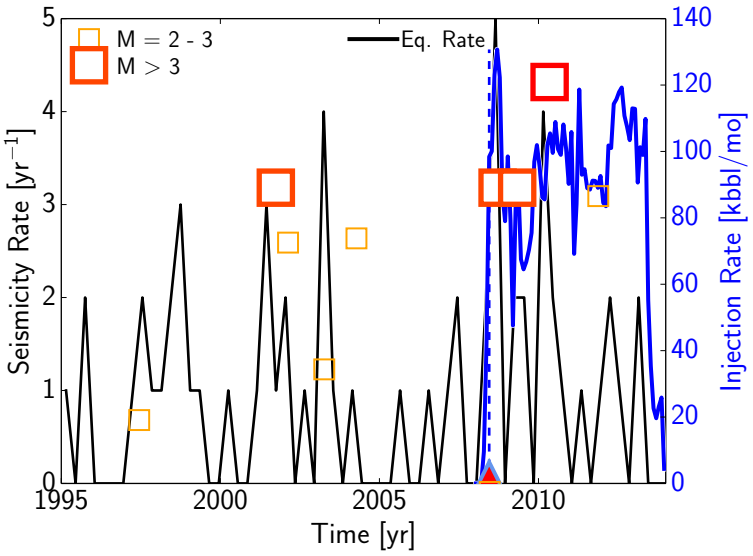

Figure 3: Injection (blue curve) and seismic activity (black curve, and frames colored according to magnitude) for one particular injection well. The two $M_{\text{L}} > 3$ events after a rapid increase in injection activity in 2010 are likely part of the background activity within the area. Based on the values of $P_{\text{ran}} = 0.16$, and $R = 0.50$ (0.46, 0.55), we consider this sequence likely not induced.

Figure 3 shows another example for which a rapid change in injection rates (here in ∼2008) is followed by two $M_{\text{L}} > 3$ earthquakes. Based on the overall observed seismic activity, we estimate values of $P_{\text{ran}} = 0.16$, and $R = 0.50$ (0.46, 0.55), indicating no significant correlation between injection and seismicity rate changes.

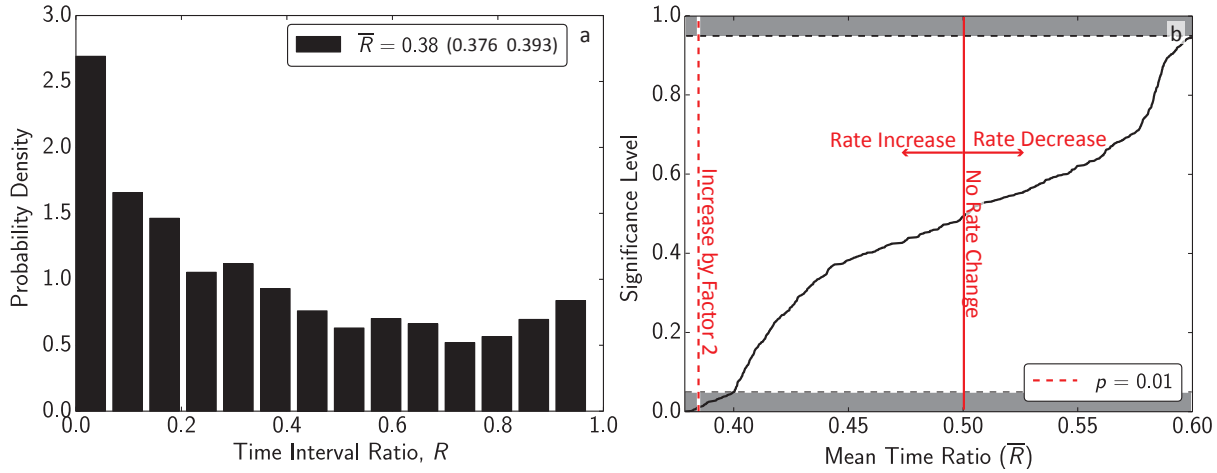

Figure 4: Left: Distribution of R-values with a mean value of $\overline{R} \approx 0.33$. The left-skewness of the distribution indicates that the trigger at time t_T strongly affected the following inter-event times and corresponding seismicity rates. Right: Cumulative distribution of all possible values for $\overline{R}$ estimated by randomly drawing t_T from the entire catalog duration. The observed $\overline{R}$-ratio falls with the first percentile of the resampled data indicating high statistical significance.

4 Characteristics of R-statistic, expected values and significance tests

The mean time interval ratio, $\overline{R}$, performed well in describing average rate changes in synthetic catalogs. In the following, we present results for time interval ratios computed from synthetic catalogs with Poissonian rate steps and main-aftershock clustering. For the simplest case, for which event origin times are normally spaced so that $\lambda_1 = 1/t_1$ and $\lambda_2 = 1/t_2$, a step increase in rate by a factor of two results in a value of $\overline{R} = 1/3$ according to: $\overline{R} = 1/(1 + \lambda_2/\lambda_1)$. If events are independent in time, i.e. earthquake occurrences can be described by a Poisson process, inter-event times follow the Poisson cumulative distribution function:

$$f(t) = \lambda \exp(-\lambda t), \tag{1}$$

and the expected value of $\overline{R}$ for a step increase in the Poissonian catalog is given by (*Van der Elst and Brodsky*, 2010):

$$E(\overline{R}) = \frac{\lambda_1 \lambda_2}{(\lambda_2 - \lambda_1)^2} \left(\frac{\lambda_1}{\lambda_2} + \ln\left(\frac{\lambda_2}{\lambda_1}\right) - 1 \right). \tag{2}$$

We determined R-values for an earthquake catalog with random, uniform spatial distribution and Poissonian seismicity rate. This rate was increased by a factor of two at time t_T and over a time interval Δt, followed by a decrease to the initial seismicity rate. The resulting R-values at time t_T are strongly skewed to the left as indication, e.g. of a strong triggering process that advance the time of post-trigger seismic events (Figure 4a). We determined the overall distribution of rate changes within the catalog by randomly drawing times between start and end of the catalog and computing the corresponding values of $\overline{R}$. Expectedly, the rate increase at time t_T falls within the first percentile of rate changes as a result of being the largest rate change within the catalog (Figure 4b). We then tested a range of step-increases in Poissonian seismicity rates from a factor of 0.5 to 2.5, and compared the results to the expected values of $\overline{R}$ based on Equ 4 (Figure 5). The results for the synthetic catalogs approximately agree with the expectation highlighting that the R-statistic performs well in detecting rate variations in Poissonian earthquake catalogs.

Besides, the tests on earthquake catalogs with Poissonian rate changes, we also created catalogs that

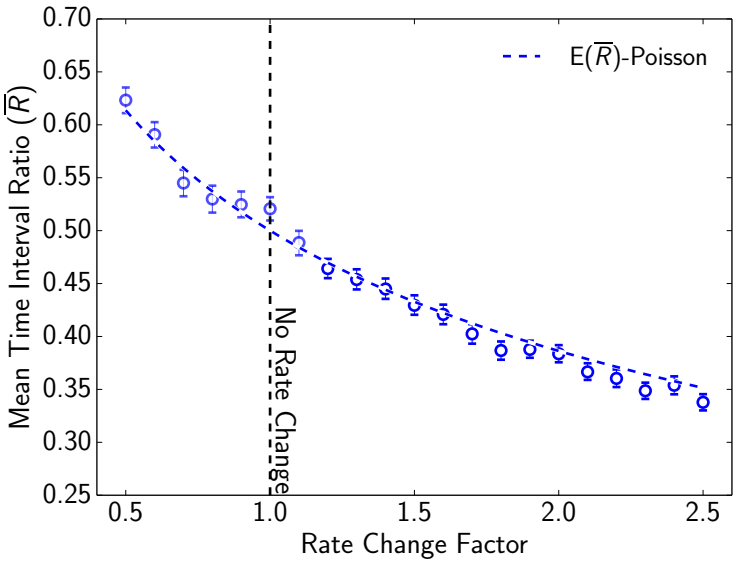

Figure 5: Time interval ratio, $\overline{R}$ (blue markers) and confidence interval (error bars) as a function of Poissonian rate increase for different synthetic seismicity catalogs. The dashed curve shows the expected values using Equ. 4.

showed spatial-temporal clustering of seismicity using an Epidemic-Type-Aftershock-Sequence (ETAS) description (*Ogata*, 1999; *Felzer et al.*, 2002; *Felzer and Brodsky*, 2006). To this end, we created aftershocks of single M4.5 events (Figure 6) but varied the aftershock productivity parameter while leaving all other parameters unchanged. Expectedly, an increase in productivity of individual aftershock sequences leads to decreasing $\overline{R}$-values (Figure 7). The aftershock catalogs with low background seismicity rates generally exhibit lower $\overline{R}$-values than catalogs with an increase in Poissonian rates. This can be explained by a relatively higher spatial-temporal density for aftershock dominated catalogs compared to catalogs that show an increase in Poissonian rates that is distributed throughout the modeled region. The results for aftershock-dominated catalogs are sensitive to the level of background seismicity rates so that high background rates can hide triggered main-aftershock sequences and $\overline{R}$-values change only marginally. In case of large aftershock productivity relative to the background rates, $\overline{R}$ decreases substantially (red markers in Figure 7). Our tests highlight that the R-statistics can reliably detects rate changes in mainshock-aftershock clustered catalogs if the background rates are low compared to the size of a particular aftershock sequence.

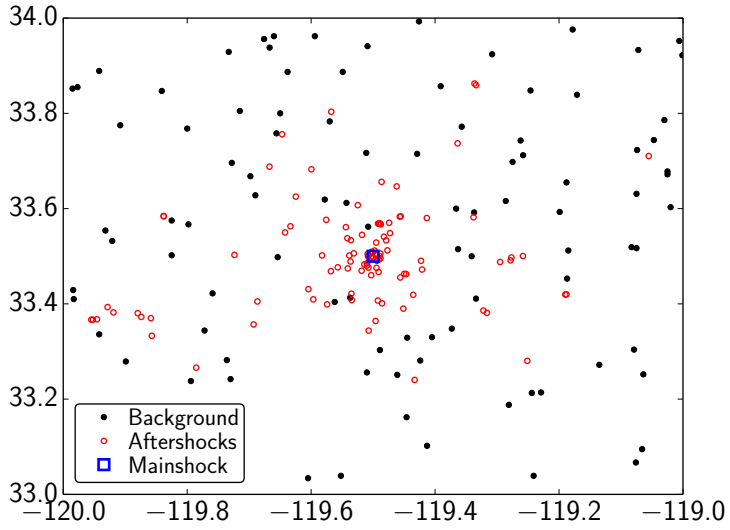

Figure 6: Example for a synthetic earthquake catalog with Poissonian background rates, and a main-aftershock sequences that is modeled by an ETAS-process

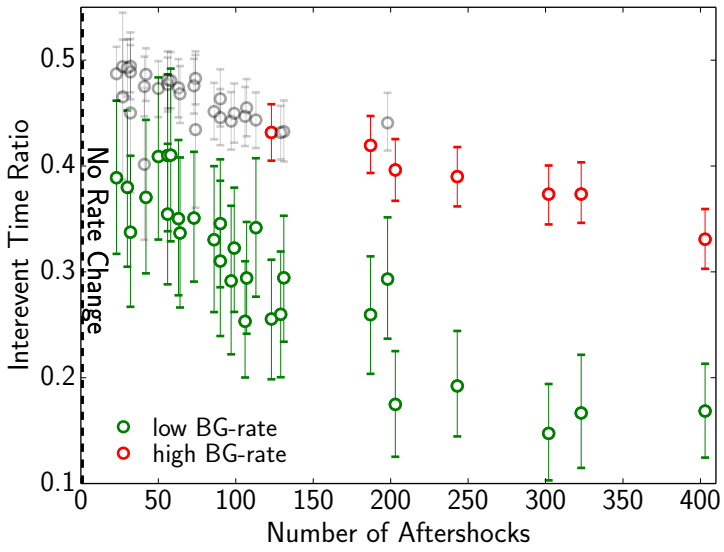

Figure 7: Inter-event time ratios for synthetic main-aftershock catalogs, and Poissonian background seismicity rates. Catalogs with relatively high background rates are highlighted by red markers, low background rates by green markers. Gray markers show catalogs without a significant rate change.

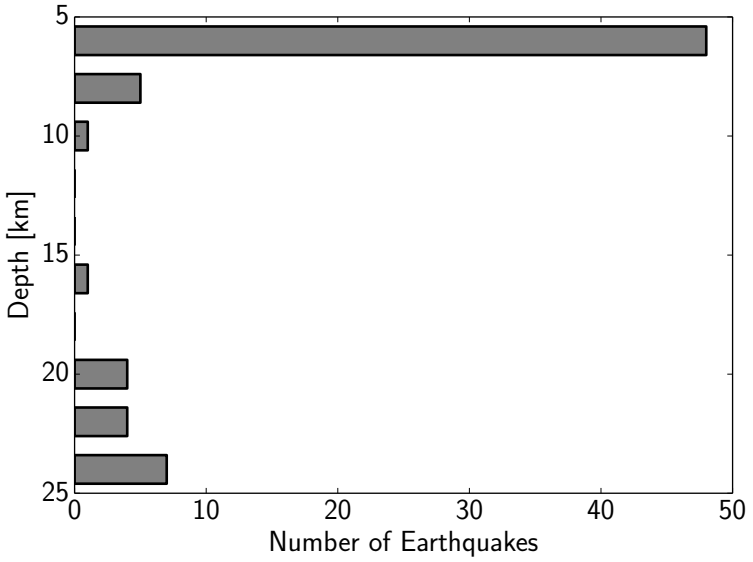

Figure 8: Histogram of earthquake depths for events associated with the *Bv* injection site between 1975 and 2013.

5 Seismicity depth distribution

The depth distribution of induced events together with the time of their occurrence relative to injection operations can provide important insights into triggering processes, and may be used to distinguish direct pore-pressure effects from elastic loading over larger distances (e.g. *Segall*, 1992; *Ellsworth*, 2013). Induced earthquakes have repeatedly been observed beneath the intended reservoir formation, with focal depths extending down to 8 km *Hsieh and Bredehoeft* (1981); *Keranen et al.* (2014); *Skoumal et al.* (2014) Thus, while focal depths may provide additional lines of evidence for possible near-injection earthquake induction, the complex processes of pore-pressure diffusion and elastic loading involve large areas and depth regimes.

The seismic record of earthquakes within the central valley provides limited information about precise focal depths as a result of very sparse station coverage. Much of the likely induced earthquake sequences show focal depths around 5 km Figures 8 to 11. We tested the depth-sensitivity of the hypocentral-inversion by artificially varying the depth between 0–20 km for each travel-time-inversion run. The resulting travel-time residuals changed only marginally highlighting the limited depth sensitivity. Generally, the closest station is located at distances corresponding to several focal depths and azimuthal gaps are large within the central valley, especially, for sites *Kr*, *Bv*, and *Lh* which are located toward the northern limit of the study area. The similar depths for most events within the ANSS-catalog can indicate earthquake induction through injection into a horizontal reservoir that contains faults close to failure. However, it may also be connected to abrupt changes in the underlying velocity models which can artificially concentrate seismicity vertically. These two possibilities are not distinguishable based on the present data set.

In contrast to *Kr*, *Lh*, *Bv*, seismicity close to injection site *Tj* is located toward the southern end of the San Joaquin basin where the seismic network density is higher. The focal depth estimates for the *Tj*05 sequence were taken from a relocated catalog (*Hauksson et al.*, 2012) and are relatively well constrained due to the presence of nearby seismic stations. The hypocenters were relocated using a 3-D velocity model and differential travel times of event clusters. While the focal depths are deeper than commonly expected for injection induced earthquakes, fluid migration along fault damage zones with relatively high permeability (e.g. *Faulkner et al.*, 2010) may facilitate pore-pressure perturbations or elastic stress variations at the observed depths. A possible candidate for a fault that may act as fluid-conduit is the Wheeler Ridge fault (see main manuscript Figure 9) which is favorably oriented between injection site

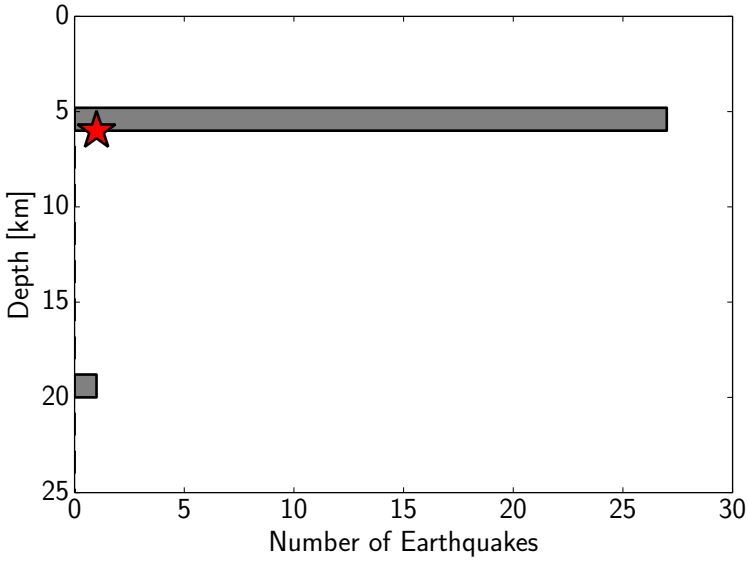

Figure 9: Histogram of earthquake depths for seismicity following a rapid increase in injection-rates close to site *Lh* in 1988. Red star highlights the mainshock depth.

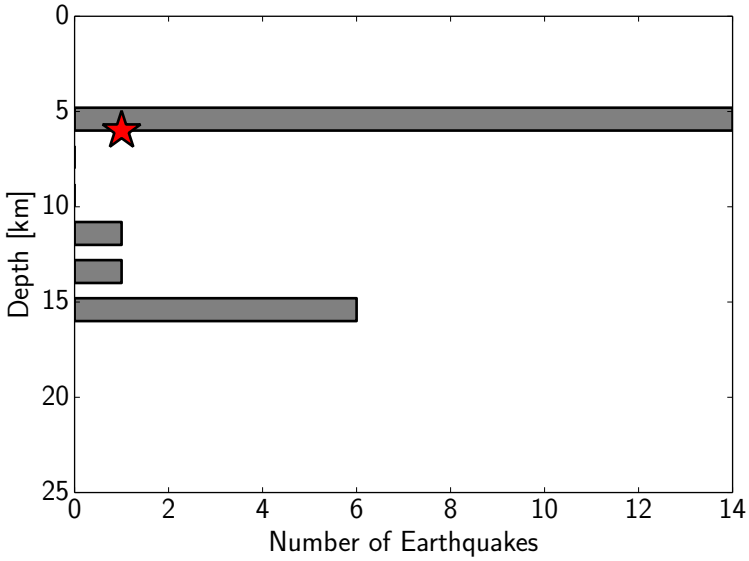

Figure 10: Histogram of earthquake depths for seismicity following a rapid increase in injection-rates close to site *Kr* in 1985. Red star highlights the mainshock depth.

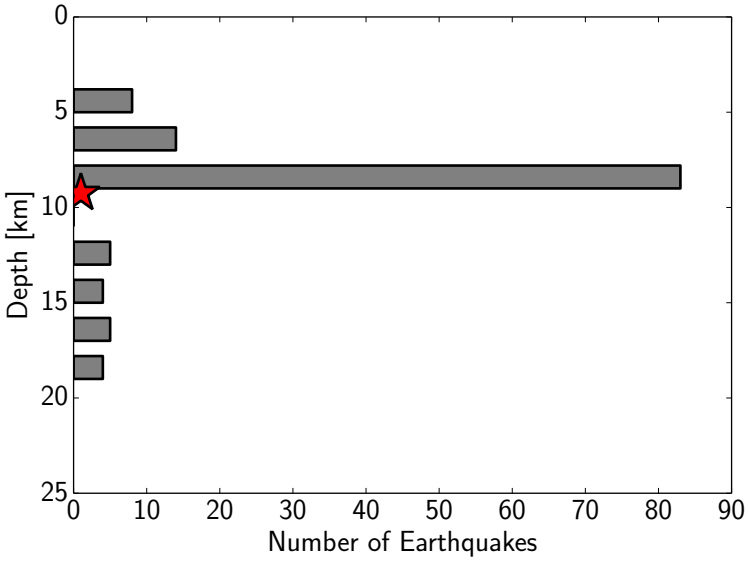

Figure 11: Histogram of earthquake depths for seismicity following a rapid increase in injection-rates close to site Tj in 2005. Red star highlights the mainshock depth.

and the mainshock location. Pore pressure perturbations at greater depth and large distance have been reported in previous studies as a result of enhanced flow along a reservoir or fault (e.g. *Keranen et al.*, 2014). For example in Colorado, a localized high-permeability reservoir was likely responsible for elevating pore-pressures and triggering seismicity at $\sim$8 km epicentral distance from injection and $\sim$8 km depth *Hsieh and Bredehoeft* (1981). These values are similar to observations close to the injection site Tj which showed seismic activity at $\sim$8 km depth and $\sim$9 km epicentral distance. The corresponding space-time window is in agreement with a diffusive process assuming a hydraulic diffusivity of $D \sim 1.0$ m^2/s.

References

Ellsworth, W. L. (2013), Injection-induced earthquakes, *Science*, *341*(6142).

Faulkner, D. R., C. A. L. Jackson, R. J. Lunn, R. W. Schlische, Z. K. Shipton, C. A. J. Wibberley, and M. O. Withjack (2010), A review of recent developments concerning the structure, mechanics and fluid flow properties of fault zones, *J. Struct. Geol.*, *32*(11), 1557–1575, doi:10.1016/j.jsg.2010.06.009.

Felzer, K. R., and E. E. Brodsky (2006), Decay of aftershock density with distance indicates triggering by dynamic stress, *Nature*, *441*, doi:10.1038/nature04799.

Felzer, K. R., T. W. Becker, R. E. Abercrombie, G. Ekström, and J. R. Rice (2002), Triggering of the 1999 Mw 7.1 Hector Mine earthquake by aftershocks of the 1992 Mw 7.3 Landers earthquake, *J. Geophys. Res.*, *107*(B9), ESE–6.

Hauksson, E., W. Yang, and P. M. Shearer (2012), Waveform relocated earthquake catalog for Southern California (1981 to june 2011), *Bull. Seism. Soc. Am.*, *102*(5), 2239–2244.

Hsieh, P. A., and J. D. Bredehoeft (1981), A reservoir analysis of the Denver earthquakes: A case of induced seismicity, *J. Geophys. Res.*, *86*(B2), 903–920.

Keranen, K., M. Weingarten, G. Abers, B. Bekins, and S. Ge (2014), Sharp increase in central Oklahoma seismicity since 2008 induced by massive wastewater injection, *Science*, *345*(6195), 448–451.

Ogata, Y. (1999), Seismicity analysis through point-process modeling:a review, *pageoph*, *155*, 471–507.

Segall, P. (1992), Induced stresses due to fluid extraction from axisymmetric reservoirs, *Pure and Applied Geophysics*, *139*(3-4), 535–560.

Skoumal, R. J., M. R. Brudzinski, B. S. Currie, and J. Levy (2014), Optimizing multi-station earthquake template matching through re-examination of the Youngstown, Ohio, sequence, *Earth Plant. Sc. Lett.*, doi:10.1016/j.epsl.2014.08.033.

Van der Elst, N. J., and E. E. Brodsky (2010), Connecting near-field and far-field earthquake triggering to dynamic strain, *J. Geophys. Res.*, *115*(B7).